Structural and Magnetic Characteristics of Polyol Synthesized Cobalt Nanoparticles with Ruthenium and Samarium Additives: A First-Order Reversal Curve Analysis

Mohammed H. Abbas
Hashim Jabbar

Department of Physics, College of Science, University of Basrah, Basra, IRAQ

As a 3*d* metal element, cobalt (Co) has been widely utilized in the synthesis of magnetic materials, inducing high magnetic anisotropy and Curie temperature. Here, a polyol method is used to synthesize Co nanoparticles (NPs) with Ru and Sm rare-earth element additives. X-ray diffraction patterns indicate the formation of different crystal structures of Co NPs with the additives, whereas field-emission scanning electron microscopic images show similar mean diameters and size distributions of the NPs with spherical-like morphology. Hysteresis loop measurements show higher coercivity (H_c= 315 Oe) and lower saturation magnetization (M_s= 84.59 emu/g) of Ru-added Co NPs compared to Sm-added Co NPs (H_c= 66 Oe and M_s= 109.94 emu/g). First-order reversal curve analysis manifests predominant single domain and superparamagnetic contributions for Ru- and Sm-added Co NPs, respectively, thereby shedding light on their different magnetic behavior at room temperature.

***Keywords*:** Magnetic nanoparticles; Ferromagnetics; Coercivity; Magnetic domains
Received: 20 December 2023; **Revised:** 29 January; **Accepted:** 05 February 2024

1. Introduction

Cobalt (Co) is considered one of ferromagnetic elements with a constant transition phase at high temperatures. This element has a high Curie temperature of approximately 1145°C, resulting from exchange interaction between 3*d* electrons. The Co atoms can be crystallized in three different forms, including hexagonal close-packed (hcp), face-centered cubic (fcc) and ε-phase structures [1]. The potential applications of Co and Co-based materials have been considered in magnetic recording media, sensors, and microwave devices. In particular, Co nanoparticles (NPs) containing rare-earth elements can provide tunable magnetic properties by adjusting their structural and morphological parameters such as crystallinity, crystal orientation and diameter, as well as shape and size [2]. In fact, magnetic properties of NPs are directly related to the crystal structure, grain size and magnetic anisotropy [3], playing an important role in magnetic characteristics such as coercivity (H_c), saturation magnetization (M_s), and remanence ratio (M_r/M_s).

The number of studies devoted to the synthesis and characterization of transition metal NPs has increased in recent years. This is due to the possible introduction of new physical properties, allowing for the acquisition and better understanding of previously unavailable information [4]. Basically, the synthesis of Co NPs via polyol methods has gained attention lately [5]. Notably, Harris et al. prepared cobalt carbide NPs with Co_2C and Co_3C phases using a polyol method. In this case, a large H_c=3kOe was obtained at room temperature (RT), resulting from high magnetic anisotropy due to the specific morphology, crystal structure, and inter-particle exchange interaction [6]. Mehdi et al. also prepared Co_2C/Co_3C powders by a modified polyol method, taking into account some factors such as the reaction temperature, reaction time, and surfactant. The results showed H_c of 2.3 kOe and M_s of more than 45 emu/g [7]. Another study investigated the formation of hybrid Co_2C and Co_3C NPs by utilizing a one-pot template free method, giving rise to H_c=0.3kOe and M_s=75.9 emu/g [8]. Qie et al. prepared long-chain amines at high temperatures using a pyrolysis method, obtaining Co_2C NPs with good crystallinity and large H_c of about 1.3 kOe [9].

Importantly, the understanding of magnetic characteristics of NPs is necessary when developing their applicability for various research purposes. In this regard, first-order reversal curve (FORC) analysis is a sophisticated technique used in the study of magnetic materials, providing detailed information about the distribution of interaction fields and coercivities. This technique is capable of revealing different magnetic domain structures such as single domain (SD), multidomain, and superparamagnetic (SP) states. In other words, FORC measurements can give extra and more detailed information about magnetic characteristics compared to hysteresis loop measurements [10,11]. Notwithstanding, less attention has been paid to FORC measurements of rare-earth element added Co NPs, according to the best of our knowledge.

In this paper, Ru and Sm rare-earth element additives are added to Co NPs synthesized using a polyol method. Carbon is also used in the synthesis process to act as a surfactant. Structural,

morphological and compositional characteristics of the resulting NPs are investigated via different techniques. Particular attention is paid to investigate magnetic behavior of Co NPs containing the rare-earth elements based on magnetic parameters obtained from hysteresis loop and FORC measurements. This study indicates the effective dependence of structural and magnetic properties on the type of rare-earth elements.

2. Experimental Part

Cobalt acetate tetrahydrate ($Co(CH_3COO)_2.4H_2O$, Merck, 99%), ruthenium(III) chloride hydrate ($RuCl_3.H_2O$, Sigma-Aldrich, 99.98%), samarium(III) chloride hexahydrate ($SmCl_3.6H_2O$ Sigma-Aldrich, 99%), NaOH (Merck, 99%), 1,2-Butanediol ($C_4H_{10}O_2$, Sigma-Aldrich, 98%), and ethanol (99.9%) were used without further purification.

Co NPs with Ru and Sm additives were synthesized using a polyol method. For the former case, 0.83g of $Co(CH_3COO)_2.4H_2O$, 0.03g of $RuCl_3.H_2O$ and 0.5g of NaOH were added into a 250mL three-neck flask containing 45mL of 1, 2-butanediol solvent.

The mixture was degassed from the first reaction under N_2 atmosphere at RT for 5 min, and then heated between 250-300°C under N_2 atmosphere and mechanical stirring for 35 min. The resultant solution was allowed to cool down at RT, followed by magnetically separating the precipitate using a permanent magnet. The collected precipitate was washed several times with ethanol, and centrifuged. Finally, the precipitate was filtered and dried at RT.

In the latter case, 0.79 g of $Co(CH_3COO)_2.4H_2O$, 0.13 g of $SmCl_3.6H_2O$, and 0.64 g of NaOH were dissolved in 65 mL of 1,2-butanediol. The mixture was heated under reflux conditions, and the above explained procedure was used to prepare the NPs. The prepared Ru and Sm-added Co NPs were attracted to a permanent magnet, indicating their magnetic nature.

Crystalline structure of Co NPs synthesized with Ru and Sm additives was investigated via x-ray diffraction (XRD, Philips X'Pert Pro) analysis with Ni-filtered Cu Kα radiation. Morphological properties were studied using field-emission scanning electron microscopy (FE-SEM, MIRA3 TESCAN). The composition and elemental mapping of the NPs were determined by energy-dispersive x-ray spectroscopy (EDS) [12,13]. Room-temperature (RT) magnetic properties of Ru- and Sm-added Co NPs were measured using hysteresis loop analysis through the utilization of a vibrating sample magnetometer (VSM, MDK, Iran) equipped with FORC software. In this respect, the maximum range of magnetic field applied to the NPs was ±6 kOe.

3. Results and Discussion

Figure (1a,b) shows XRD patterns of Ru- and Sm-added Co NPs, respectively, indicating the formation of different crystal structures. From Fig. (1a), the peaks observed at 2θ of 42.1°, 44.8°, 47.8°, 62.7° and 76.1° correspond to (100), (002), (101), (102) and (110) planes, respectively, of "hcp" Co structure with lattice constants (a=b= 2.5031Å, c=4.0605Å) and angles (α=β=90°, γ=120°) (JCPDS card no. 00-005-0727).

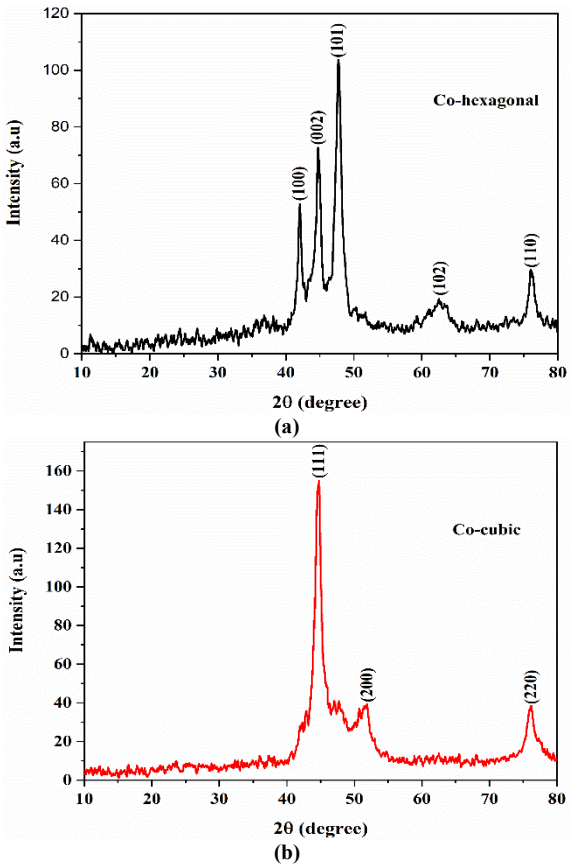

Fig. (1) XRD patterns of Co NPs synthesized with rare-earth element additives (a) Ru and (b) Sm

From Fig. (1b), the peaks at 2θ of 44.7°, 51.4° and 76.1° can be ascribed to (111), (200) and (220) planes, respectively, indicating the formation of "fcc" Co structure with lattice constants (a=b=c=3.5447Å) and angles (α=β=γ=90°) (JCPDS card no. 00-015-0806). Therefore, it is possible to change the crystal structure of Co NPs, depending on the rare-earth element type. It is worth noting that the XRD patterns cannot reveal the presence of Ru and Sm elements due to their small amount (acting as additives) in the synthesis of Co NPs.

The average crystallite size (D) of the NPs was calculated using Scherrer's equation given below [14,15]:

$$D = \frac{K\lambda}{\beta \cos\theta} \quad (1)$$

where K is the shape factor, λ is the x-ray wavelength, β is the full-width at half maximum, and θ is the diffraction angle

The results obtained are presented in table (1). As observed, the crystallite size of Co NPs with Ru and

Sm additives is found to be 17.40 and 13.02 nm, respectively.

Table (1) Structural and morphological characteristics of Co NPs synthesized using Ru and Sm additives

Additive	Crystallite size (nm)	Mean diameter of NPs (nm)	Standard Deviation
Ru	17.40	28.71	6.39
Sm	13.02	27.31	5.05

Figure (2a,b) depicts FE-SEM images of Co NPs synthesized in the presence of Ru and Sm additives, indicating spherical-like morphology with mean diameters of 28.71 and 27.31 nm, respectively. These images also exhibit some agglomeration and seeding clusters, arising from the involvement of the rare-earth elements. In turn, the formation of larger particles observed in the images may be assigned to the seeding of cobalt grains by the rare-earth elements. The corresponding NP size distribution histograms are shown in Fig. (3). As can be seen, while the mean diameter of Ru- and Sm-added Co NPs is similar to each other, the latter shows a wider NP size distribution induced by the Sm additive.

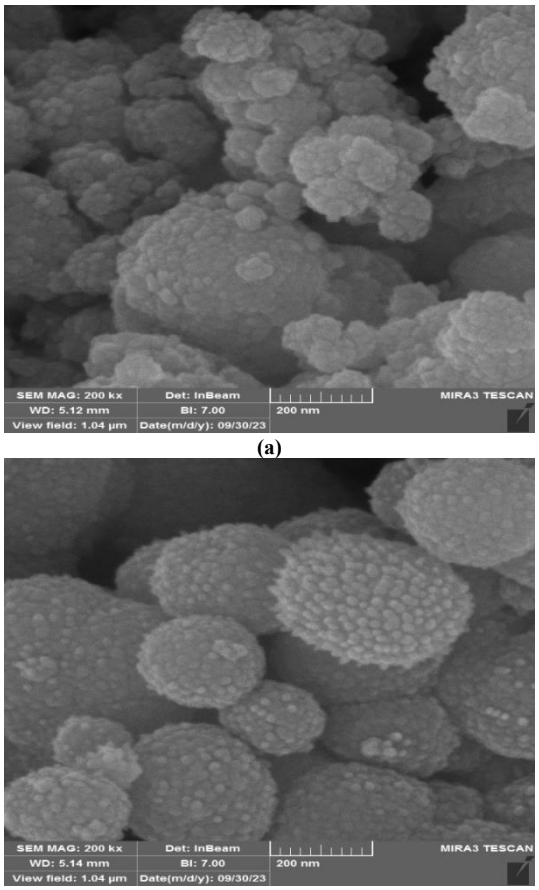

Fig. (2) FE-SEM images of Co NPs synthesized with rare-earth element additives (a) Ru and (b) Sm

The EDS spectra of Co NPs synthesized in the presence of the rare-earth element additives are shown in Fig. (4). From Fig. (4a), the presence of Co, C and Ru elements with atomic percentages of 67.02%, 31.43% and 1.55% is observed. Based on Fig. (4b), the EDS spectrum shows atomic percentages of 83.77%, 15.51% and 0.72% for Co, C and Sm elements. Overall, the EDS spectra evidence the additive role of the rare-earth elements in Co NPs. It should be noted that the small amount of C element with the binding energy of 0.28 keV in the Co NP composition arises from the solvent used in the synthesis reaction (1,2-butanediol), leading to the binding of Co with C atoms so as to form cobalt carbide. On the other hand, the elemental mapping of the Ru- and Sm-added Co NPs is depicted in Fig. (5). As inferred, the distribution of Ru and Sm rare-earth element additives is uniform across the NP samples.

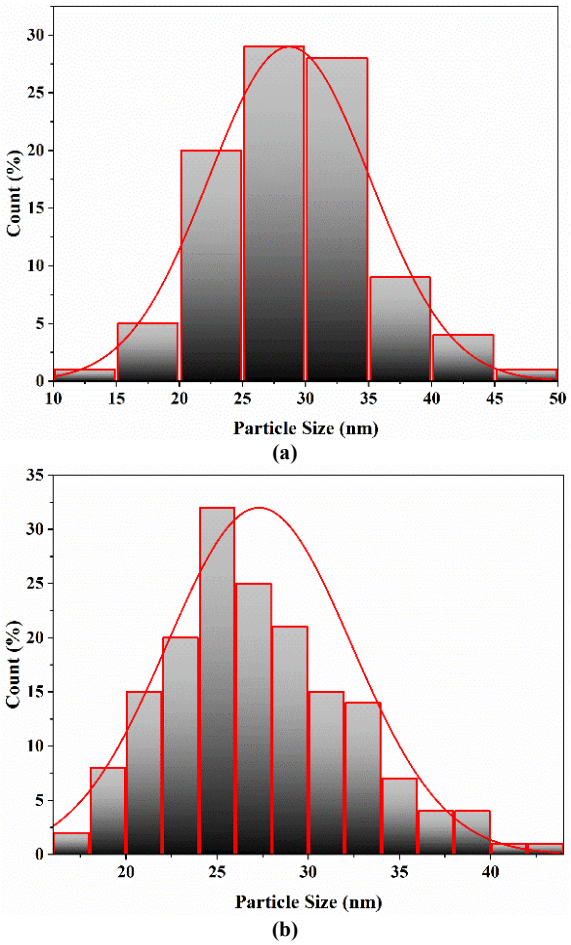

Fig. (3) Nanoparticles size distribution histograms of (a) Ru- and (b) Sm-added Co NPs extracted from FE-SEM images

Figure (6) shows RT hysteresis loops of Ru- and Sm-added Co NPs, together with the corresponding switching field distribution (SFD) curves measured under an external magnetic field of ±6 kOe, while the hysteresis loop of Ru-added Co NPs shows a relatively high H_c value, the narrow hysteresis loop of Sm-added Co NPs is indicative of considerably lower H_c and higher M_s values. Quantitatively, table (2) presents magnetic parameters (including H_c, M_r, M_s, and M_r/M_s) extracted from the hysteresis loop measurements. In this regard, H_c and M_s values of Co NPs synthesized in the presence of Ru and Sm

additives are found to be 315 Oe and 84.59 emu/g, and 66 Oe and 109.94 emu/g, respectively. Essentially, the higher H_c of Ru-added Co NPs may arise from their stronger magnetic anisotropy. To calculate the magnetic anisotropy constant (K) from hysteresis loop measurements, the following equation can be used [16,17]:

$$K = \frac{M_S H_C}{0.96} \quad (2)$$

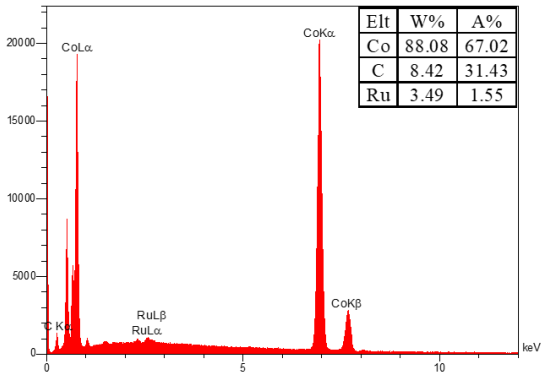

(a)

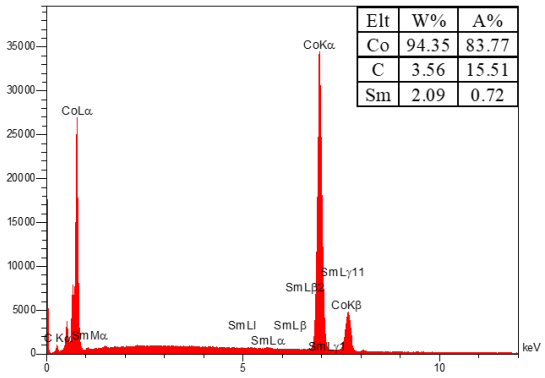

(b)

Fig. (4) EDX spectra of Co NPs synthesized with rare-earth element additives (a) Ru and (b) Sm

Also, it is possible to calculate the energy product of magnetic NPs using the following equation:

$$(BH)_{Max} = \frac{M_r H_C}{16\pi} \quad (3)$$

The SFD can be calculated as follows:

$$SFD = \frac{\Delta H}{H_c} \quad (4)$$

where ΔH is taken at the half maximum peak of SFD curve. As a crucial value of magnetic recording media, S^* is determined by the following equation:

$$\left.\frac{dM}{dH}\right|_{H_C} = \frac{M_r}{H_C(1-S^*)} \quad (5)$$

where dM/dH is the slope at H_c, and M_r is the remanence magnetization [18]

Table (2) presents the results calculated from the above-mentioned equations for the Co NPs with the rare-earth element additives. Clearly, the higher H_c of Ru-added Co NPs is justified by their considerably larger K (27756.75 erg/g) compared to that for Sm-added Co NPs (K=7558.65 erg/g). Meanwhile, $(BH)_{max}$ and S^* of Ru-added Co NPs is larger (1148.06 GOe and 0.33), which make them suitable for magnetic recording media. Basically, non-interacting SD NPs with uniaxial orientation are expected to have M_r/M_s of 0.5, according to Stoner-Wohlfarth model [19]. Herein, M_r/M_s of Ru and Sm-added NPs is found 0.22 and 0.07, indicating their magnetically interacting behavior that can be investigated using FORC analysis.

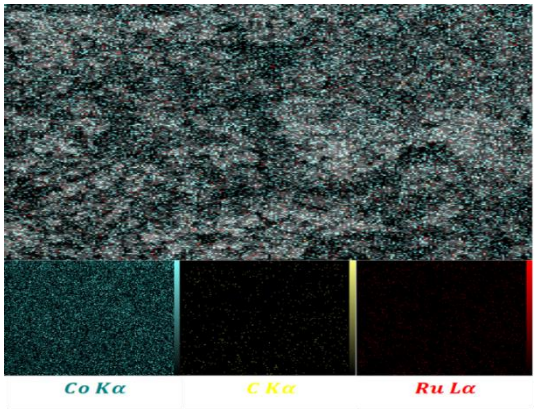

(a)

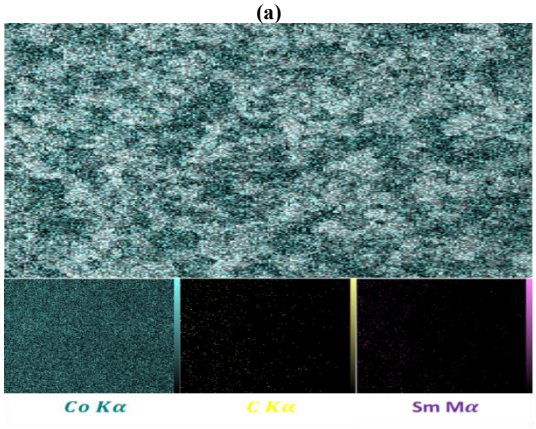

(b)

Fig. (5) Elemental mapping of Co NPs synthesized with rare-earth element additives (a) Ru and (b) Sm at the range of 5 µm

FORC analysis is performed by applying an external magnetic field (H) sufficient to magnetically saturate the NP sample. Next, the magnetic field is reduced to a reversal field (H_r), while also measuring magnetization M (H, H_r). In this way, sets of FORCs are acquired. To obtain the distribution of FORC, ρ (H, H_r), the equation given below is utilized [20]:

$$\rho(H, H_r) = -\frac{1}{2}\frac{\partial^2 M(H,H_r)}{\partial H \partial H_r} \quad (6)$$

The FORC diagram can be plotted with colors ranging from blue (minimum of ρ) to red (maximum of ρ). Also, the coercive field (H_c) and interaction field (H_u) axes are described as follow [21]:

$$H_c = \frac{H - H_r}{2} \quad (7)$$

$$H_u = \frac{H + H_r}{2} \quad (8)$$

Figure (7) displays FORC diagrams along with sets of FORCs obtained for Ru- and Sm-added Co NPs. Figure (7a) shows a tear-drop configuration in the FORC diagram, involving a broad distribution of coercive field with two peaks. For better clarity, figure (8a) shows the corresponding coercive field distribution (CFD). As observed, the first peak of

distribution is positioned around the origin of the FORC diagram. This peak reflects the involvement of magnetically soft Co NPs with FORC coercivity of about zero (H_C^{FORC}~ 0 Oe). The second distribution is broadened along the H_c axis, indicating the presence of magnetically harder NPs with H_C^{FORC}= 364 Oe. According to the results of hysteresis loop measurements, H_c of Ru-added Co NPs was 315 Oe, approximating the corresponding H_C^{FORC} value for the magnetically harder phase. This, in turn, indicates that SD NPs plays the dominant role in magnetic characteristics of the NPs. Note that the lower hysteresis loop H_c compared to H_C^{FORC} is due to the presence of the magnetically softer NPs, thereby decreasing the overall H_c value.

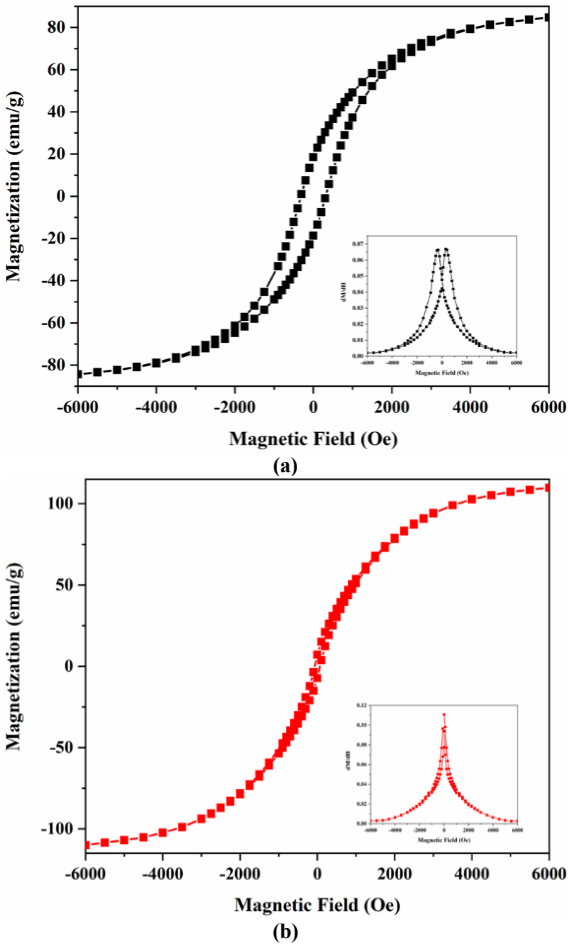

Fig. (6) Room-temperature hysteresis loops of Co NPs synthesized using (a) Ru and (b) Sm as additives. The insets show the corresponding SFD curves measured under an applied field of ±6 kOe

Figure (7b) shows FORC diagram of Sm-added Co NPs. As can be observed, the FORC distribution is mostly positioned around the origin of the diagram with a high density of 9.99×10^{-7} (see Fig. 8a), indicating that SP NPs play the key role in determining the overall magnetic properties [22]. This predominant SP contribution might be the reasoning behind the higher M_s of Sm-added Co NPs (109.94 emu/g) compared to Ru-added Co NPs (84.59 emu/g). In other words, the enhanced susceptibility of SP NPs may lead to an increase in M_s [23]. On the other hand, the SP NPs show weak magnetic interactions (ΔH_u= 298 Oe), as evidenced from their narrow distribution along the H_u axis (see Fig. 8b) and table 3).

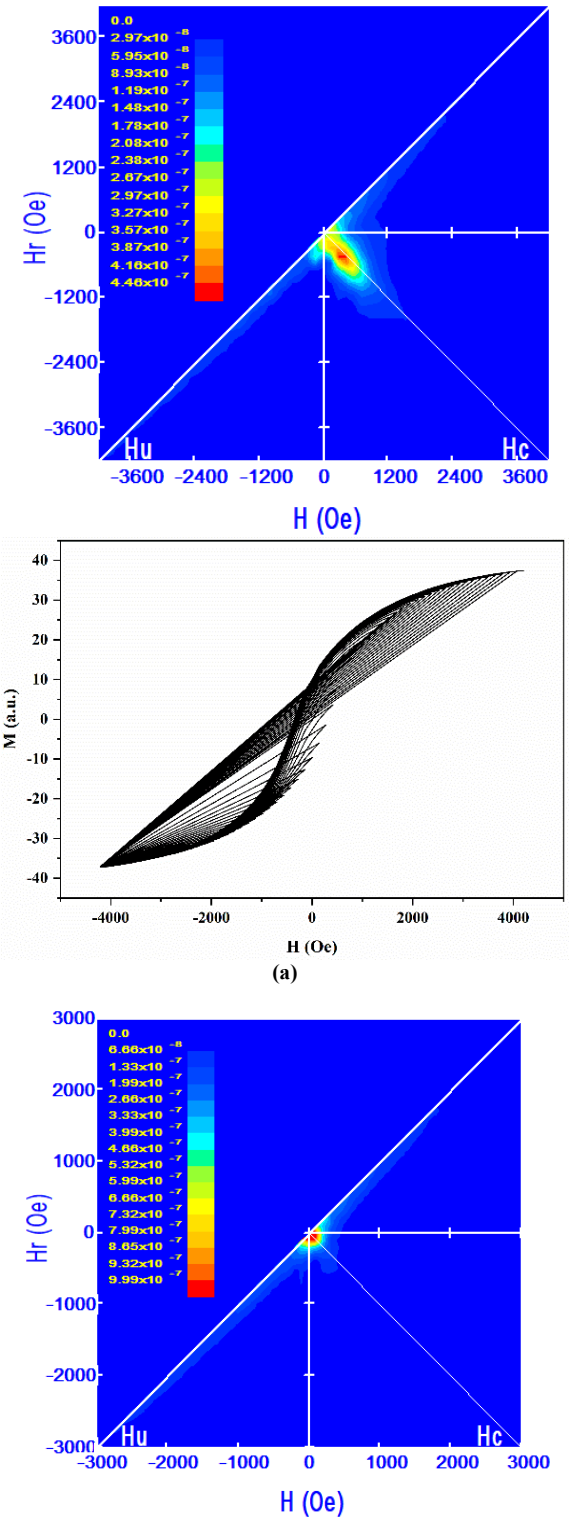

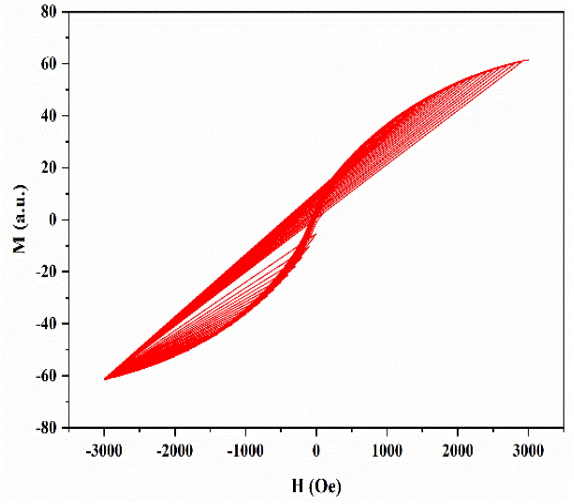

(b)

Fig. (7) FORC diagrams along with sets of FORCs obtained for Co NPs synthesized with rare-earth element additives (a) Ru and (b) Sm

Table (3) Magnetic characteristics of Ru- and Sm-added Co NPs extracted from FORC measurements

Additive	ΔH_u (Oe)	Rev. (%)	Irr. (%)	SP Fraction (%)
Ru	1221	55	45	10
Sm	298	72	27	45

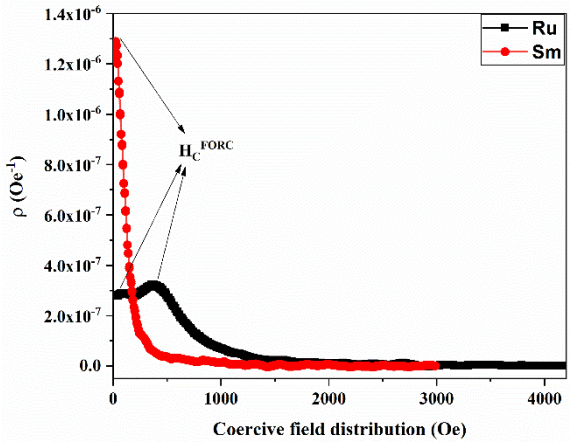

(a)

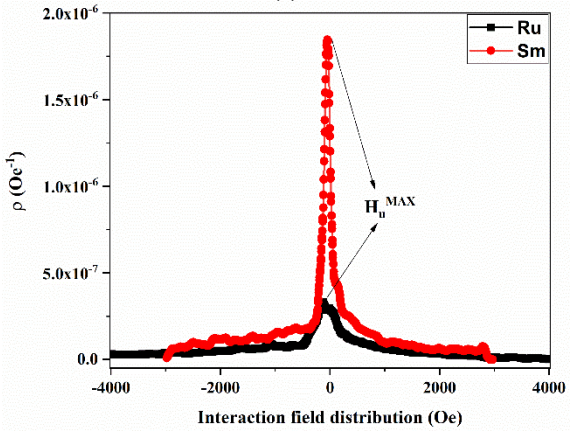

(b)

Fig. (8) (a) Coercive field distribution (CFD) and (b) interaction field distribution (IFD) for Co NPs synthesized with Ru and Sm additives

Finally, the reversible and irreversible parts (hysteresis loops) of magnetization were extracted from FORC measurements, and the results obtained are shown in Fig. (9). From Fig. (9a), the reversible fraction of Ru-added Co NPs is found to be 55%, whereas that of Sm-added Co NPs significantly increases to 72%. This remarkable enhancement in the reversible fraction is due to the SP contribution of NPs. Therefore, it is estimated that SP fraction is 45%, as presented in table (3).

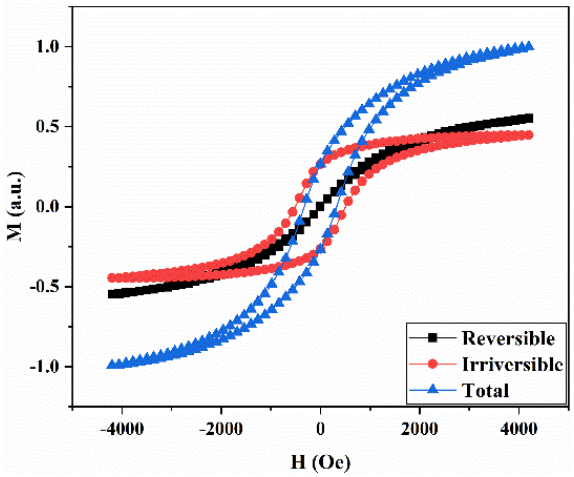

(a)

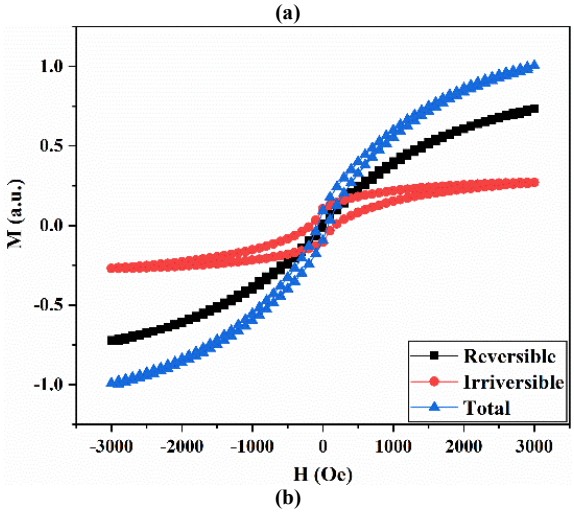

(b)

Fig. (9) Reversible, irreversible and total hysteresis loops extracted from FORC measurements of Co-NPs synthesized with (a) Ru and (b) Sm additives

4. Conclusion

Ru and Sm rare-earth elements have been utilized to act as additives in the synthesis of Co NPs using a polyol method. The results showed crystallite sizes of 17.40 and 13.02 nm for Ru- and Sm-added Co NPs, arising from hcp and fcc crystal structures, respectively. They also showed uniform distribution of the additives in the Co NPs, involving 1.55% and 0.72% contents for Ru and Sm elements, respectively. The results indicated the main role of SD and SP contributions in determining magnetic properties of Ru- and Sm-added Co NPs, so that the H_c of the former (315 Oe) was higher than that of the latter (66 Oe). In this regard, SP fraction of Co NPs with weak

magnetic interactions was estimated to be 45%, resulting from the significant reversible part of magnetization. Meanwhile, the dominant SP contribution induced a considerably higher M_s (109.94 emu/g) for Sm-added Co NPs compared to that for Ru-added Co NPs (84.59 emu/g).

References

[1] J. Mohapatra et al., "Hard and semi-hard magnetic materials based on cobalt and cobalt alloys", *J. Alloys Comp.*, 824 (2020) 153874.
[2] A. Esmaeili et al., "Tailoring magnetic properties in arrays of pulse-electrodeposited Co nanowires: The role of Cu additive", *J. Magn. Magn. Mater.*, 397 (2016) 64-72.
[3] X. Shen et al., "A facile one-pot method for synthesis of single phase Co_2C with magnetic properties", *Mater. Lett.*, 271 (2020) 127783.
[4] A.F. Khusnuriyalova et al., "Preparation of Cobalt Nanoparticles", *Euro. J. Inorg. Chem.*, 2021 (2021) 3023-3047.
[5] R.J. Joseyphus et al., "Designed synthesis of cobalt and its alloys by polyol process", *J. Solid State Chem.,* 180 (2007) 3008-3018.
[6] V.G. Harris et al., "High coercivity cobalt carbide nanoparticles processed via polyol reaction: A new permanent magnet material", *J. Phys. D: Appl. Phys.,* 43 (2010) 165003.
[7] M. Zamanpour et al., "Magnetic properties and scale-up of nanostructured cobalt carbide permanent magnetic powders", *J. Appl. Phys.*, 115(17) (2014) A747.
[8] Z. Chen, L. Liu and Q. Chen, "One-pot template-free synthesis of urchin-like Co_2C/Co_3C hybrid nanoparticles", *Mater. Lett*., 164 (2016) 554-557.
[9] Y. Qie et al., "High coercivity cobalt carbide nanoparticles as electrocatalysts for hydrogen evolution reaction", *Nano Res*., 15 (2022) 3901-3906.
[10] A.R. Muxworthy, J.G. King and D. Heslop, "Assessing the ability of first-order reversal curve (FORC) diagrams to unravel complex magnetic signals", *J. Geophys. Res. Solid Earth*, 110 (2005) 1-11.
[11] A.P. Roberts et al., "Understanding fine magnetic particle systems through use of first-order reversal curve diagrams", *Rev. Geophys.*, 52 (2014) 557-602.
[12] S.M.S. Al-Khazali, H.S. Al-Salman and A. Hmood, "Low cost flexible ultraviolet photodetector based on ZnO nanorods prepared using chemical bath deposition", *Mater. Lett.*, 277 (2020) 128177.
[13] N.A. Abdullah, B. Ali and H. Jabbar, "Study the Effect of TiO_2 Nanoparticles in Multilayers of Photoelectrode Prepared by Ball Milling Technique on the Performance of Dye Sensitized Solar Cells (DSSCs)", *IOP J. Phys.: Conf. Ser.*, 1818 (2021) 012069.
[14] A.S. Abed, S.J. Kasim and A.F. Abbas, "Optical and Structural Properties of CdS Quantum Dots Synthesized Using (MW-CBD) Technique", *Iraqi J. Nanotechnol.,* 1 (2020) 44-52.
[15] M.M. Ali, S.J. Abbas and A.S. Al-Kabbi, "Influence of annealing temperature on the properties of ZnO nanostructures", *Basrah J. Sci.,* 73 (2019) 356-375.
[16] E. Fantechi et al., "Influence of cobalt doping on the hyperthermic efficiency of magnetite nanoparticles", *J. Magn. Magn. Mater*., 380 (2015) 365-371.
[17] R.C. Kambale et al., "Effect of cobalt substitution on structural, magnetic and electric properties of nickel ferrite", *J. Alloys Comp.*, 478 (2009) 599-603.
[18] F. Kalil and A. Buschman, **"High-Density Digital Recording"**, NASA Reference Publication (1985).
[19] M.F. De Campos et al., "Stoner-wohlfarth model for the anisotropic case", *J. Magn. Magn. Mater.,* 345 (2013) 147-152.
[20] D. Heslop and A.P. Roberts, "Estimation of significance levels and confidence intervals for first-order reversal curve distributions", *Geochem. Geophys. Geosyst.*, 13(5) (2012) 1-12.
[21] A.R. Yasemian, M. Almasi Kashi and A. Ramazani, "Hyperthermia properties of $Ni_xFe_{3-x}O_4$ nanoparticles: a first-order reversal curve investigation", *J. Mater. Sci.: Mater. in Electron.*, 30 (2019) 21278-21287.
[22] A.P. Roberts, C.R. Pike and K.L. Verosub, "First-order reversal curve diagrams: A new tool for characterizing the magnetic properties of natural samples", *J. Geophys. Res. Solid Earth,* 105 (2000) 28461-28475.
[23] M. Kumari et al., "Distinguishing magnetic particle size of iron oxide nanoparticles with first-order reversal curves", *J. Appl. Phys.*, 116 (2014) 124304.

Table (2) Magnetic characteristics of Ru- and Sm-added Co NPs extracted from hysteresis loop measurements

Additive	H_c (Oe)	M_r (emu/g)	M_s (emu/g)	M_r/M_s	K (erg/g)	$(BH)_{MAX}$ (GOe)	SFD	S*
Ru	315	18.56	84.59	0.22	27756.75	1148.06	4.76	0.33
Sm	66	7.20	109.94	0.07	7558.65	93.24	13.56	0.28

